Instrumented cardiac microphysiological devices via multimaterial three-dimensional printing

Instrumented cardiac microphysiological devices via multi-material 3D printing

Authors
Johan U. Lind[1,2,4], Travis A. Busbee[1,2,4], Alexander D. Valentine[1,2], Francesco S. Pasqualini[1,2], Hongyan Yuan[1,2,3], Moran Yadid[1,2], Sung-Jin Park[1,2], Arda Kotikian[1,2], Alexander P. Nesmith[1,2], Patrick H. Campbell[1,2], Joost J. Vlassak[2], Jennifer A. Lewis[1,2]*, Kevin K. Parker[1,2]*

[1] Wyss Institute for Biologically Inspired Engineering,
Harvard University, Boston, MA 02115 USA

[2] John A. Paulson School of Engineering and Applied Sciences,
Harvard University, Cambridge, MA, 02138 USA

[3] Current Affiliations: Department of Mechanical, Industrial and Systems Engineering,
University of Rhode Island, Kingston, RI, 02881 USA

[4] These authors contributed equally to this work

*Correspondence should be addressed to:
Kevin Kit Parker
29 Oxford St.
Cambridge, MA 02138
Phone: (617) 495-2850
Fax: (617) 495-9837
E-mail: kkparker@seas.harvard.edu

Jennifer A. Lewis
29 Oxford St.
Cambridge, MA 02138
Phone: (617) 496-0233
Email: jalewis@seas.harvard.edu

Biomedical research has relied on animal studies and conventional cell cultures for decades. Recently, microphysiological systems (MPS), also known as *organs-on-chips*, that recapitulate the structure and function of native tissues *in vitro* have emerged as a promising alternative[1]. However, current MPS typically lack integrated sensors and their fabrication requires multi-step lithographic processes[2]. Here, we introduce a facile route for fabricating a new class of instrumented cardiac microphysiological devices via multi-material 3D printing. Specifically, we designed six functional inks, based on piezo-resistive, high conductance, and biocompatible soft materials that enable integration of soft strain gauge sensors within micro-architectures that guide the self-assembly of physio-mimetic laminar cardiac tissues. We validated that these embedded sensors provide non-invasive, electronic readout tissue of contractile stresses, inside cell incubator environments. We further apply these devices to study drug responses, as well as the contractile development of human stem cell derived laminar cardiac tissues over four weeks.

Current MPS models of muscle tissue rely on microscopy coupled with optical tracking analysis for assessing tissue contractile stress. For instance, muscular thin film (MTF) assays track changes in curvature of soft cantilever substrates induced by the contraction of a laminar tissue [3], and micro-post assays measure the deflection of pillars supporting a micro-tissue [4]. Although these assays have proven valuable for short-term modeling of human disease and small-scale drug screening applications [1, 5, 6], they are not well suited for higher throughput or longer term studies. Moreover, biomimetic microsystems are currently fabricated using soft-material lithography-based techniques that require multiple steps, masks and dedicated tools[4, 7-9], which hinders rapid prototyping and customization. By contrast, multi-material 3D

printing of viscoelastic inks enables a wide range of functional, structural and biological materials to be patterned and integrated in a single programmable manufacturing step [10-14].

Here, we introduce a fully 3D printed and instrumented microphysiological device that provides continuous electronic readout of the contractile stress of multiple laminar cardiac micro-tissues (Fig. 1a-b). Each device contains three key features: *i)* multilayer cantilevers, composed of a base layer, an embedded strain sensor, and a tissue-guiding layer, *ii)* electrical interconnects for readout, and *iii)* eight independent wells (Fig. 1c-i). The tissue-guiding layer promotes self-assembly of engineered physio-mimetic laminar tissues from neonatal rat ventricular myocytes (NRVMs) and human induced pluripotent stem cell derived cardiomyocytes (hiPS-CMs). Our microphysiological device facilitates tissue culture and non-invasive analyses of tissue contractile strength over several weeks, and facilitates drug studies inside a controlled incubator environment.

To create this integrated device, six materials are patterned sequentially via direct ink writing multi-material 3D printing. To allow material integration at the microscale, the substrate topology and *x-y-z* positions of four individually addressable nozzles are determined by an automated calibration process (see supplementary movie S1). After this calibration, the device is printed in a single continuous procedure (Fig. 1c-i and supplementary movies S2-3).

The stress generated by laminar cardiac tissues is limited to 1-15kPa [5, 8]. Hence, to match this range, both the thickness and stiffness of each cantilever layer must be minimized. Towards this objective, we designed a series of highly dilute polymer-based inks. Their low solids content ensures patterning of thin individual layers (0.5 – 6.5μm in thickness). Additionally, by tuning the evaporation rate of the carrier solvent solution, the ink viscosity and corresponding wetting and spreading behavior is controlled to achieve the desired lateral

dimensions (supplementary Fig. S1-2). Using these inks, we first printed 0.5μm dextran films (Fig. 1c), which serve as biocompatible, water-soluble sacrificial release layers that allow the final cantilevers to detach from the substrate and deflect freely. Next, using dilute thermoplastic polyurethane (TPU) inks, 3μm thick cantilever bases, 6.5μm thick strain gauge wires and 1.5 μm thick wire covers are printed in steps 2-4, respectively (Fig. 1d-f). The cantilever base and wire covers are printed using an unfilled TPU ink, while the strain gauge wires are printed using a TPU ink filled with 25wt% carbon black nanoparticles (CB:TPU). The printed TPU-based features exhibited elastic mechanical properties with Young's modulus of 1.6MPa (supplementary Fig. S3), while CB:TPU features readily cured to form an elastic piezo-resistive material with Young's modulus of 8.8MPa and resistivity of 1.19Ω·cm (supplementary Fig. S3-7). Several alternative fillers were investigated, including metals particles [15] and carbon nanotubes[16]. However, we found that carbon black imparts the best combination of ink rheology, low stiffness and sensor hysteresis.

The remainder of the microphysiological device is printed using concentrated viscoelastic inks optimized for deposition of self-supporting structures (supplementary Fig. S8-9). Using a soft viscous PDMS ink (Young's modulus of 1.28MPa, see Supplementary Fig. S3), ~60μm wide filaments are patterned on top of each cantilever (Fig. 1g). These comprised the majority of the cantilever thickness and served as direct support below the physio-mimetic laminar cardiac tissue. Next, electrical leads and contact pads are printed using a high-conductivity, silver particle-filled, polyamide (Ag:PA) ink (Fig. 1h). Upon drying, the printed wires exhibit an electrical resistivity of 6.6×10^{-5}Ω·cm (supplementary Fig. S4), which ensures that the primary electrical resistance of the final device arose from the embedded CB:TPU strain gauges. Finally, the wire leads are covered with an insulating layer and eight individually addressable wells are

printed using either a PDMS ink or biocompatible rigid thermoplastic polymers such as polylactid acid (PLA) or acrylonitrile butadiene styrene (ABS). The rigid polymers can be preferable for drug study applications, as they are less prone to bulk absorption of hydrophobic drugs than PDMS [17] (Fig. 1i, supplementary Fig. S10). After printing, the devices are cured at 100℃ and subsequently seeded with cardiomyocytes, which self-assemble into laminar tissues mimicking the structure of the native heart.

The musculature of the heart is composed of highly organized, structurally and electrically anisotropic layers [18]. To recapitulate this architecture *in vitro*, we printed a range of grooved microstructures by varying the spacing between curved ~20μm x 60μm (height x width) filaments and assessed their ability to guide the self-assembly of anisotropic laminar NRVM tissues (Fig. 2). We evaluated the degree of tissue structural anisotropy using immunofluorescent imaging of sarcomeric α-actinin and quantification of the sarcomere Orientational Order Parameter (OOP) (Fig. 2a-f, supplementary Fig. S11) [19]. All substrates showed an OOP > 0.2 indicative of non-random sarcomere alignment. The highest OOP ~0.5 was observed for 60μm filament spacing. Similarly, 60μm filament spacing gave rise to the highest degree of electrophysiological anisotropy in the laminar NRVM tissues (Fig. 2g-i, supplementary Movies S4-7). For this spacing, action potential propagation was 2.7 times faster parallel to the grooves compared to the transverse direction. These data are in agreement with the longitudinal to transverse velocity ratio of 2.1 observed in the native ventricle [18]. Also, these anisotropic laminar tissues gave rise to unidirectional and concerted cantilever deflection and displayed the highest contractile stresses in the final devices (supplementary Fig. S12-14). Collectively, these results demonstrate that our printing technique can be employed to engineer laminar cardiac tissues with a range of ordered architectures. Notably, the OOP and

electrophysiology data closely matched values obtained using semi-manual micro-contact printing and molding techniques [7, 20].

To accurately measure the stress exerted by the physio-mimetic laminar cardiac tissues, the embedded strain gauges within each cantilever must produce a reliable and detectable signal. We therefore evaluated the electro-mechanical properties of CB:TPU in a series of uniaxial strain tests (Fig. 3a-d, supplementary Fig. S5-7). To mimic the strains exerted by tissue contraction, 1-3Hz triangular strains of 0.1% were applied to CB:TPU gauges. In this strain range, the gauges displayed a linear strain-resistance relationship with limited hysteresis and a corresponding gauge factor of 2.51±0.09. In order to accurately convert resistance signals to stresses generated by the laminar cardiac tissues, we established a mechanical model of the cantilevers based on a multilayer version of Stoney's equation (Fig. 3e-f and supplementary information). The mechanical model relies on the dimensions and Young's moduli of each layer of the cantilever as well as the CB:TPU gauge factor. The model provides linear conversion factors between the relative changes in gauge resistance, changes in cantilever radius of curvature, and in turn, the longitudinal stresses generated by the laminar cardiac tissues. Applying these conversion factors, we obtained tissue twitch stress (σ_{twitch}), the differences between the systolic and diastolic stress, in the range of 7-15kPa for laminar NRVM tissues, akin to prior reports [3, 7]. To further verify the model, we compared the sensor readout with stress values concurrently obtained through optical tracking of cantilever deflection, and obtained highly similar stress values (Fig. 3g-h, supplementary Fig. S12-14, supplementary Movie S8-11). Yet, we observed one discrepancy between the optical tracking and electrical readout: at the initiation of tissue contraction, a small decrease in gauge resistance is seen, prior to the increase caused by cantilever deflection. We attribute this decrease to a brief axial compression of the

gauge wire occurring during initial tissue contraction, while cantilever deflection is counteracted by inertial and viscous forces. Notably, this observation does not influence tissue twitch stress values. Together, these results demonstrate that the CB:TPU strain-gauges embedded in our fully printed platform provide reliable readouts of tissue contractile stress.

Data acquisition from cardiac microphysiological systems based on optical readout is laborious, requires dedicated microscopy setups, semi-automated image analysis software, and is limited by the image readout file sizes [4, 5]. By contrast, our fully printed and instrumented cardiac devices provide a direct, non-invasive electronic readout of contractile stresses. Therefore, we could perform dose response studies of drugs that influence contraction strength or beat rate, directly inside a cell incubator, an ideal *in vitro* environment (Fig. 3i-j, supplementary Fig. S15-18). As examples, we carried out cumulative drug dose studies with the L-type calcium channel blocker verapamil and the β-adrenergic agonist isoproterenol. For laminar NRVM tissues we observed a negative inotropic response to verapamil, with an apparent EC_{50} of $1.15x10^{-6}$M when paced at 1Hz (Fig. 3i). We also observed a negative chronotropic effect for spontaneously beating tissues (supplementary Fig. S17), in good agreement with prior studies on isolated postnatal whole rat hearts [21]. Similarly, we observed a positive chronotropic response to isoproterenol for spontaneously beating laminar tissues, matching previous studies of engineered NRVM micro-tissues [4] (supplementary Fig. S18). For hiPS-CM-based laminar tissues, we observed a positive inotropic response to isoproterenol, with an apparent EC_{50} of $2.69x10^{-9}$M when paced at 2Hz (Fig. 3j), resembling studies based on embryonic stem cell derived cardiomyocyte tissue [22].

Beyond facilitating acute drug studies, our platform is well suited for extended studies to identify gradual changes in the contractile stress of engineered cardiac tissues, which can occur

over the course of multiple weeks [22, 23]. As a demonstration, we studied the *in vitro* contractile development of laminar tissues based on hiPS-CMs over the course of 28 days (Fig. 4a-g). During this period, the longitudinal contractile stress initially increased 4-fold from day 2 to 4, followed by a more gradual increase (Fig. 4a-b). Similarly, the spontaneous beating rate decreased (Fig. 4c), indicative of increased maturity [24]. The changes in twitch stress are mirrored by a structural development of the laminar hiPS-CM tissues (Fig. 4d-g, supplementary Fig. S19). From day 2 to day 14 the sarcomere OOP increased from 0.11 to 0.32 (Fig. 4e), while the Sarcomere Packing Density (SPD, a measure of sarcomere periodic organization) increased from 0.07 to 0.2 (Fig. 4f), indicating that hiPS-CMs undergo sarcomerogenesis and myofibrillogenesis during culture [19]. Importantly, from day 14 to day 28, a significant increase in sarcomere length from 1.7μm to 1.8μm was observed (Fig. 4g), indicative of a more mature tissue [25].

While traditional muscular thin films mimic essential features of the cardiac architecture, cell-cell contacts are confined to a single cell layer. By contrast, a number of *in vitro* cardiac tissue models composed of thicker micro-tissues have been reported [26-28]. To illustrate the versatility of our 3D printing methodology, we modified the MPS device to support thicker micro-tissues, approximately 4 cell layers thick (supplementary Fig. S21-24). This thickness matches that of the myocyte layers in a mammalian heart (i.e., ~ 4 cells in thickness per layer, each layer separated by connective tissue) [29]. To balance the increased contractile stress and mitigate tissue delamination, we printed thicker cantilevers that contained ~100 μm tall micro-pin arrays with tunable areal density (Fig. 4h-i, supplementary movie S13-15). Despite these modifications to both the cardiac tissue and cantilevers, the tissue remains orders of magnitude softer than the substrate. Hence, the basic assumptions of the mechanical model remain valid,

and the sensor signal is directly proportional to mean tissue stress (see supplementary information). We carried out proof of principle isoproterenol and verapamil drug studies to illustrate the functional relevance of these thicker NRVM based tissues (Fig. 4j-k). We observed the expected positive and negative inotropic responses with apparent EC_{50} values comparable to earlier data from engineered 3D NRVM tissues and isolated postnatal whole rat hearts [21, 28].

Through multi-material 3D printing of a series of customized inks, we demonstrated the automated design and fabrication of instrumented cardiac microphysiological devices. The integrated sensors drastically simplify data acquisition and long term functional studies. Leveraging the ability to track the temporal development in tissue mechanics will enable new insights into tissue morphogenesis, pathogenesis, and drug-induced structural and functional remodeling. Our digital manufacturing approach is quite versatile, allowing for fabrication of a range of instrumented microphysiological devices. Notably, our approach facilitates rapid customization to match device geometries, mechanical and biochemical properties to a specific diseased state or a unique patient derived cell source. Our programmable microfabrication approach opens new avenues for *in vitro* tissue engineering, toxicology and drug screening research.

Methods

Ink formulations

The following ink formulations were used: *Dextran ink*: 10g/ml Dextran (Sigma-Aldrich) was dissolved in 9:1 v:v, water: isopropanol, *TPU ink*: TPU 15wt% Elastollan 35A (BASF) dissolved in 4:1 v:v tetrahydrofuran:dimethylformamide, *CB:TPU ink*: TPU 15wt% Elastollan 35A, 5wt% carbon black (Vulcan XC72R, Cabot) dissolved in 4:1 v:v tetrahydrofuran:dimethylformamide. *Ag:Pa ink*: 50g Silver flakes (5-8μm) mixed with 5.2g 30wt% versamid 973 solution (BASF) dissolved in pentanol, mixed with an additional 2.72g of pentanol. *Soft PDMS Ink*: SE1700 (Dow-Corning) with1:25 curing agent based ratio was applied for cantilever covers, micro-pins and micro-wells. *Rigid PDMS ink*: SE1700 (Dow-Corning), with 1:10 curing agent weight ratio, mixed 1:5 wt:wt with Sylgard 184 1:10 curing agent weight ratio (Dow-Corning) is used for wells and covers, or as gasket adhesive below PLA or ABS wells and covers.

Print procedure with integrated profiling

Printing was carried out using a three-axis motion-controlled stage (Aerotech) with 4 independent z-axes. Prior to printing, a custom automation system was applied to determine the substrate topology and relative x-y-z nozzle positions using an integrated laser profilometer, three CCD micrometers (Keyence), and custom machined fixtures. G-code generation and custom automation scripts were programmed using open-sourced python libraries (Mecode). Extrusion was carried out using syringes, dispense tips, and a digital pneumatic regulator (EFD). Dispense tip diameters: *TPU ink*: 100μm, *CB:TPU ink*: 200μm, *Ag:PA ink*: 250μm, *Soft PDMS ink*: 30μm, *Rigid PDMS ink*: 410μm. For Dextran ink a refillable contact-pressure sensitive pen (0.7mm tip, Montana) was utilized as deposition nozzle.

Device cell seeding and culture

Prior to cell seeding, devices were sterilized by UV-Ozone exposure for 8mins. Subsequently, wells were incubated with a 50μg/ml solution of Fibronectin (BD biosciences) in PBS for 1hr. Fibronectin solution was aspirated and wells seeded with either primary NRVMs at a seeding density of a seeding density of 140k/cm^2 in 10% FBS in media 199 (Life Technologies) or hiPS-CMs (Cor4U, Axiogenesis, Germany) at 220k/cm^2 in designated Commercial Cor4U media (Axiogenesis, Germany). For thicker tissue version, NRVM are seeded at 1M/cm^2 adding cold BD Matrigel^{TM} (BD biosciences) to final concentration 0.45-0.6mg/ml, thus below gelling concentration. NRVMs were acquired from Sprague Dawley rats (*n≥10 litters, per harvest*) applying procedures approved by the Harvard University Animal Care and Use Committee, described in detail in supplementary information. hiPS-CMs were thawed, pre-plated and seeded following guidelines from supplier, as detailed in supplementary information. Cell media was changed at least every second day, applying 2% FBS in media 199 (Life Technologies) for NRVM culture, and designated Cor4U media for hiPS-CM culture.

Data acquisition

Data collection was performed using custom machined holder connecting device to a Keithley Multichannel DMM 3706a. Readouts were obtained either as 2-wire resistance recordings sampling at ≥60Hz. A custom MATLAB *(MathWorks, Natick, MA)* code was applied for quantifying relative resistance changes upon tissue contraction applying peak detection and comparison with local baseline, for electrically paced samples a median filter (5) was applied. Linear conversion constants between relative resistance change, cantilever curvature and stress generated by tissue, were established using designated mechanical model.

Isoproterenol and verapamil Cumulative drug dose studies

Cumulative dosing of isoproterenol or verapamil (Sigma-Aldrich) cardiac drugs was performed on laminar NRVM and hiPS-CM tissues inside incubator. 700ul serum free media was added to each well prior to drug dose experiments. A dilution series of the drugs in media (Life Technologies) was sequentially added in 7ul doses. Tissue was incubated for 10mins for each dose, prior to recording. For each dose at least 30s were recorded per channel. Isoproterenol stocks were kept at 4℃ prior to dosing. Pacing was applied using custom platinum wire electrodes. Each *n* denotes separate device wells with isolated tissue, sensor and media.

Tissue immuno-staining and structural analysis

All immunocytochemistry procedures were conducted at room temperature. Samples were first fixed with 4% PFA/PBS (v/v) solution for 15mins and then permeabilized with 0.05 % Triton-X/PBS (v/v) solution for 10mins. Subsequently, samples were incubated for 1hr with a monoclonal sarcomeric α-actinin (clone EA-53; Sigma-Aldrich) primary antibody, washed three times in PBS, and finally counterstained with: Alexa Fluor 488-conjugated anti-mouse secondary antibody, Alexa Fluor 633-conjugated Phalloidin and DAPI (Invitrogen). Samples were imaged using confocal microscopy, acquiring projected Z-stack images of the wavy laminar tissues. The alignment and overall spatial organization of α-actinin positive structures in the immunostained digital images were evaluated with custom MATLAB *(MathWorks, Natick, MA)* code as previously described [19].

Optical mapping experiments to determine tissue electrophysiology

AP propagation velocities for the engineered NRVM cardiac tissues were monitored using a modified tandem-lens macroscope *(Scimedia, Costa Mesa, CA)* equipped with a high speed camera *(MiCAM Ultima, Scimedia, Costa Mesa, CA*), a plan APO 1X objective, a collimator

(Lumencor, Beaverton, OR) and a 200mW Mercury lamp *(X-Cite exacte, Lumen Dynamics, Canada*). After 4 days culture *in vitro*, 10mmx10mm engineered laminar NRVM tissues were incubated with 4μM solution of a photovoltaic dye, RH237. (Invitrogen, Carlsbad, CA) for 5mins at 37 ºC, and rinsed with Tyrode's solution prior to recording. Recordings were acquired at a frame rate of 200 Hz. Electrical point simulation was applied to the corner of the tissue using two U-shaped platinum electrodes *(Sigma-Aldrich, St. Louis, MO)* located 0.5-1mm above the tissue, applying 1-2Hz, 5-10V pulses of 10ms duration using a pulse generator *(MyoPacer Cell Stimulator, IonOptix, Milton, MA*). Post-processing of data was conducted with custom MATLAB *(MathWorks, Natick, MA)* code as previously described [30]. A spatial filter with 3 × 3 pixels was applied to improve the signal-noise ratio similar. Activation time was calculated as the average time to maximum upstroke slope of pulses when continuously paced at 2Hz during in a 5s recording window.

Statistical analysis

For analysis of tissue SPD, OOP and sarcomeric length, One Way Analyses for Variance between the compositional groups were conducted using SigmaPlot (v12.0, Systat Software Inc.). All data sets passed Shapiro-Wilk normality tests and equal variance tests. For pairwise comparison Holm-Sidak method was applied. For all statistical analyses, p-values less than 0.05 were considered statistically significant. Sample sizes were chosen based on previous studies applying muscular thin film assays [19, 20, 30].

Code availability

Custom MATLAB scripts for signal detection and stress calculation can be found as supplementary information.

Acknowledgements

The authors thank Lori K. Sanders for her work on photography and time-lapse movies, Joss A. Goss for assistance with fabrication of device holder and Jack Minardi for his development of mecode, and his help with machine automation. This work was performed in part at the Center for Nanoscale Systems (CNS), a member of the National Nanotechnology Infrastructure Network (NNIN), which is supported by the National Science Foundation under NSF award no. ECS-0335765. CNS is part of Harvard University; This work was also supported by the National Center For Advancing Translational Sciences of the National Institutes of Health under Award Number UH3TR000522, the U. S. Army Research Laboratory and the U. S. Army Research Office under Contract No. W911NF-12-2-0036, and the Harvard University Materials Research Science and Engineering Center (MRSEC) award no. DMR-1420570. The views and conclusions contained in this document are those of the authors and should not be interpreted as representing the official policies, either expressed or implied, of the Army Research Office, Army Research Laboratory, the U.S. Government, or the the National Institutes of Health. The U.S. Government is authorized to reproduce and distribute reprints for Government purposes notwithstanding any copyright notation hereon.

Competing Financial Interests

The authors declare no competing financial interests

Author Contributions

J.U.L., T.A.B, J.A.L. and K.K.P designed the study. J.U.L. and T.A.B. designed device. T.A.B. coded 3D-print procedure and automation. J.U.L, T.A.B, A.K., and A.D.V. developed and characterized the printable materials. J.U.L, A.D.V. and T.A.B, optimized and printed devices. P.H.C. performed NRVM harvest and prepared culturing media. J.U.L., M.Y. and A.P.N. performed NRVM culture, drug-dose experiments, and data analysis. M.Y. and J.U.L. conducted hiPS-CM culture, experiments and data analysis. F.S.P and J.U.L. performed tissue staining, confocal imaging, and O.O.P. analysis. S-J.P., J.U.L. conducted optical mapping experiments and analysis. H.Y. and J.J.V. developed mechanical model of device. J.U.L, T.A.B., J.A.L, and K.K.P prepared illustrations and wrote manuscript. F.S.P and A.D.V contributed to manuscript.

References

1. Bhatia, S.N. and D.E. Ingber, *Microfluidic organs-on-chips.* Nature biotechnology, 2014. **32**(8): p. 760-772.
2. Mammoto, A., et al., *Control of lung vascular permeability and endotoxin-induced pulmonary oedema by changes in extracellular matrix mechanics.* Nature communications, 2013. **4**: p. 1759.
3. Feinberg, A.W., et al., *Muscular thin films for building actuators and powering devices.* Science, 2007. **317**(5843): p. 1366-70.
4. Boudou, T., et al., *A microfabricated platform to measure and manipulate the mechanics of engineered cardiac microtissues.* Tissue Engineering Part A, 2011. **18**(9-10): p. 910-919.
5. Wang, G., et al., *Modeling the mitochondrial cardiomyopathy of Barth syndrome with induced pluripotent stem cell and heart-on-chip technologies.* Nature medicine, 2014. **20**(6): p. 616-623.
6. Hinson, J.T., et al., *Titin mutations in iPS cells define sarcomere insufficiency as a cause of dilated cardiomyopathy.* Science, 2015. **349**(6251): p. 982-986.
7. Agarwal, A., et al., *Micropatterning Alginate Substrates for In Vitro Cardiovascular Muscle on a Chip.* Advanced Functional Materials, 2013. **23**(30): p. 3738-3746.
8. Grosberg, A., et al., *Ensembles of engineered cardiac tissues for physiological and pharmacological study: Heart on a chip.* Lab on a Chip, 2011. **11**(24): p. 4165-4173.
9. Park, S.-J., et al., *Phototactic guidance of a tissue-engineered soft-robotic ray.* Science, 2016. **353**(6295): p. 158-162.
10. Lewis, J.A., *Direct ink writing of 3D functional materials.* Advanced Functional Materials, 2006. **16**(17): p. 2193-2204.
11. Hardin, J.O., et al., *Microfluidic Printheads for Multimaterial 3D Printing of Viscoelastic Inks.* Advanced Materials, 2015. **27**(21): p. 3279-3284.
12. Sun, K., et al., *3D Printing of Interdigitated Li-Ion Microbattery Architectures.* Advanced Materials, 2013. **25**(33): p. 4539-4543.
13. Miller, J.S., et al., *Rapid casting of patterned vascular networks for perfusable engineered three-dimensional tissues.* Nature materials, 2012. **11**(9): p. 768-774.
14. Kolesky, D.B., et al., *Three-dimensional bioprinting of thick vascularized tissues.* Proceedings of the National Academy of Sciences, 2016. **113**(12): p. 3179-3184.
15. Matsuhisa, N., et al., *Printable elastic conductors with a high conductivity for electronic textile applications.* Nature communications, 2015. **6**.
16. Lipomi, D.J., et al., *Skin-like pressure and strain sensors based on transparent elastic films of carbon nanotubes.* Nature nanotechnology, 2011. **6**(12): p. 788-792.
17. Berthier, E., E.W. Young, and D. Beebe, *Engineers are from PDMS-land, Biologists are from Polystyrenia.* Lab on a Chip, 2012. **12**(7): p. 1224-1237.
18. Kléber, A.G. and Y. Rudy, *Basic mechanisms of cardiac impulse propagation and associated arrhythmias.* Physiological reviews, 2004. **84**(2): p. 431-488.
19. Pasqualini, F.S., et al., *Structural Phenotyping of Stem Cell-Derived Cardiomyocytes.* Stem cell reports, 2015. **4**(3): p. 340-347.
20. Feinberg, A.W., et al., *Controlling the contractile strength of engineered cardiac muscle by hierarchal tissue architecture.* Biomaterials, 2012. **33**(23): p. 5732-5741.

21. Ošťádalová, I., et al., *Early postnatal development of contractile performance and responsiveness to Ca 2+, verapamil and ryanodine in the isolated rat heart.* Journal of molecular and cellular cardiology, 1993. **25**(6): p. 733-740.
22. Zhang, D., et al., *Tissue-engineered cardiac patch for advanced functional maturation of human ESC-derived cardiomyocytes.* Biomaterials, 2013. **34**(23): p. 5813-5820.
23. Zimmermann, W.H., et al., *Three-dimensional engineered heart tissue from neonatal rat cardiac myocytes.* Biotechnology and bioengineering, 2000. **68**(1): p. 106-114.
24. Reiser, P.J., et al., *Human cardiac myosin heavy chain isoforms in fetal and failing adult atria and ventricles.* American Journal of Physiology-Heart and Circulatory Physiology, 2001. **280**(4): p. H1814-H1820.
25. Lundy, S.D., et al., *Structural and functional maturation of cardiomyocytes derived from human pluripotent stem cells.* Stem cells and development, 2013. **22**(14): p. 1991-2002.
26. Nunes, S.S., et al., *Biowire: a platform for maturation of human pluripotent stem cell-derived cardiomyocytes.* Nature methods, 2013. **10**(8): p. 781-787.
27. Xiao, Y., et al., *Microfabricated perfusable cardiac biowire: a platform that mimics native cardiac bundle.* Lab on a Chip, 2014. **14**(5): p. 869-882.
28. Zimmermann, W.-H., et al., *Tissue engineering of a differentiated cardiac muscle construct.* Circulation research, 2002. **90**(2): p. 223-230.
29. LeGrice, I.J., et al., *Laminar structure of the heart: ventricular myocyte arrangement and connective tissue architecture in the dog.* American Journal of Physiology-Heart and Circulatory Physiology, 1995. **269**(2): p. H571-H582.
30. Sheehy, S.P., et al., *Quality metrics for stem cell-derived cardiac myocytes.* Stem cell reports, 2014. **2**(3): p. 282-294.

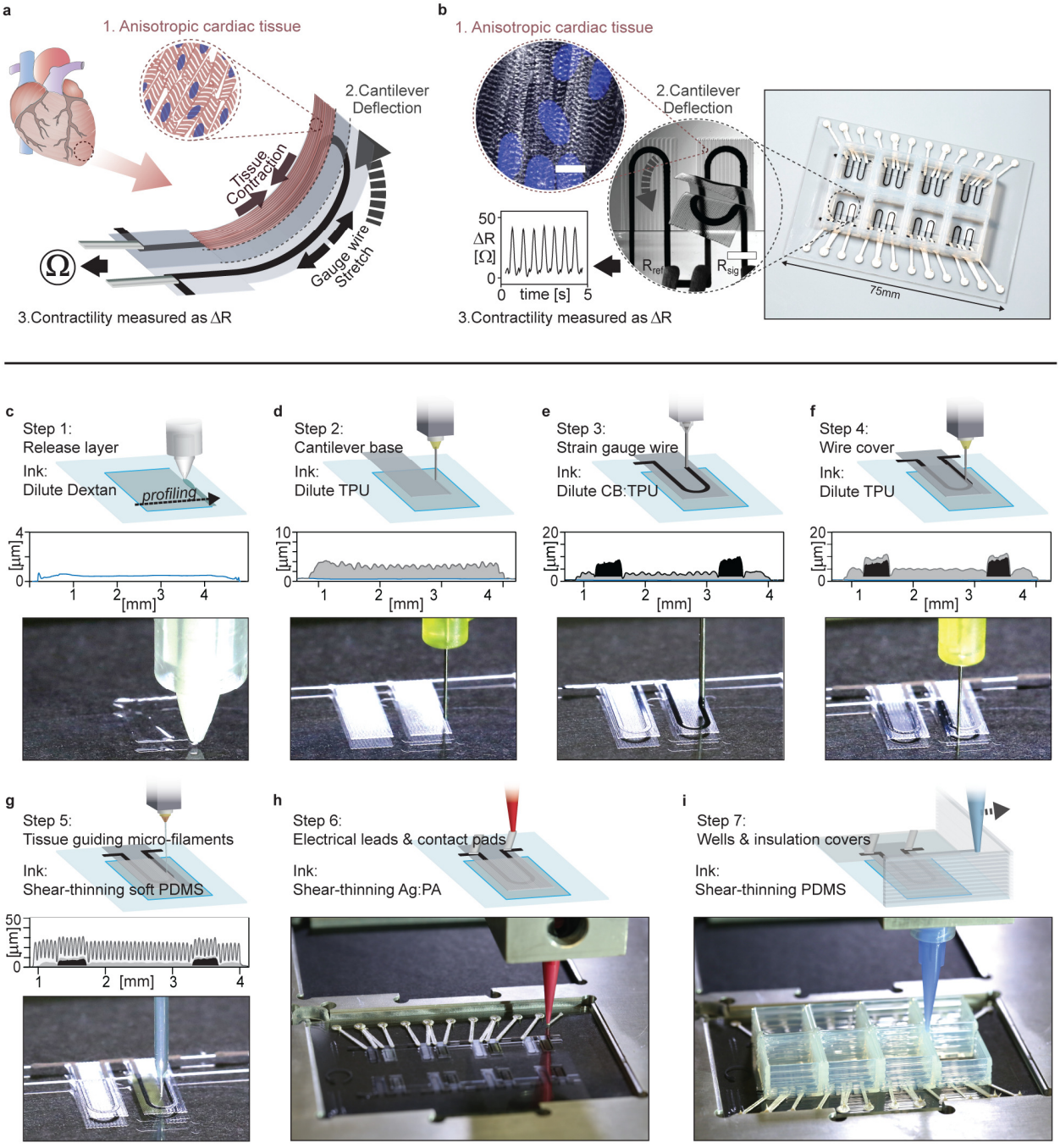

Figure 1 | Device principle and microscale 3D-printing procedure. **(a)** Principle sketch of the device. Contraction of an anisotropic engineered cardiac tissue (1) deflects a cantilever substrate (2), thereby stretching a soft strain gauge embedded in the cantilever. This generates a resistance change proportional to the contractile stress of the tissue (3). **(b)** The fully printed final device. Insert 1: Confocal microscopy image of immuno-stained laminar NRVM cardiac tissue on the

cantilever surface. Blue: DAPI nuclei stain, White: α-actinin, scale bar 10μm. Insert 2: Still images of a cantilever deflecting upon tissue contraction. Insert 3: Example resistance signal. **(c-i)** Automated printing of the device on a 2" x 3" glass slide substrate in 7 sequential steps. For each step, a corresponding still image from the printing procedure is displayed. For steps 1-5, a stylus profiling cross-sectional contour of the cantilever is additionally displayed. **(c)** In print step 1, a 0.5μm Dextran thin film sacrificial layer is printed **(d)** In print step 2**,** a 3μm TPU thin film cantilever base is printed **(e)** In print step 3, a 6.5μm thick CB:TPU strain sensor loop is added to cantilever base. **(f)** In print step 4, a 1.5μm TPU wire cover is added. **(g)** In print step 5, 20μm tall, 60μm wide PDMS micro-filaments are printed in slightly overlapping lines. The filaments constitute the top part of the cantilever and guide cardiomyocytes to form anisotropic laminar tissues. **(h)** In print step 6, electrical leads and contact are added using a high conductivity Ag:PA ink **(i)** In print step 7, covers to insulate exposed wires and wells to contain cells and media are printed using PDMS, PLA or ABS (See supplementary Fig S10).

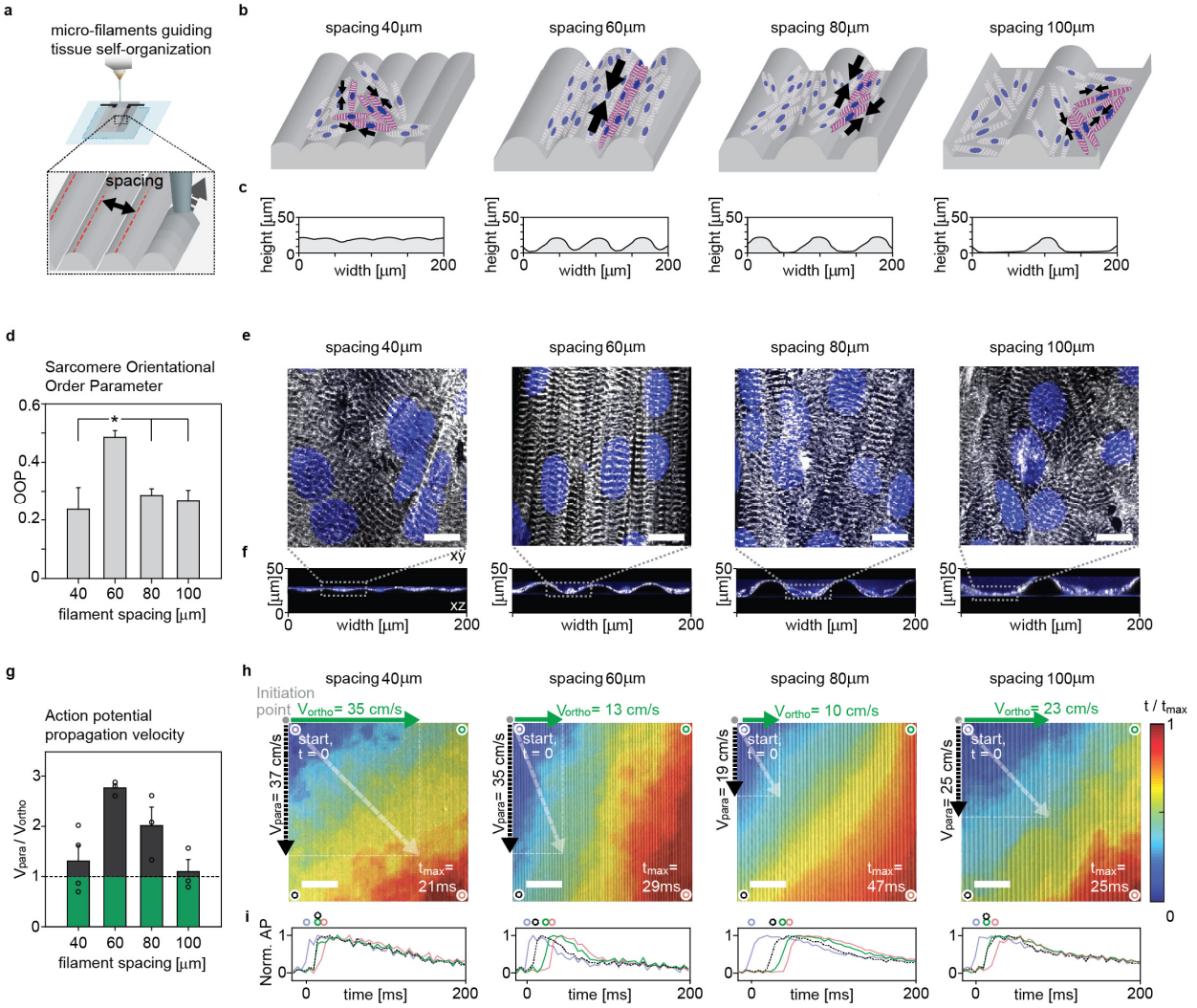

Figure 2 | Micro-grooves guide cardiomyocyte self-assembly into anisotropic engineered tissues. (a) Spacing of soft PDMS microfilaments **(b)** Sketch of micro-filaments guiding self-assembly of engineered cardiac tissue. **(c)** Stylus profilometer contours of substrates with filaments printed at 40, 60, 80 and 100µm spacing **(d)** Sarcomere OOP of laminar NRVM tissues developed on substrates with 40 (n=9), 60 (n=13), 80 (n=8) and 100µm (n=10) filament spacing, error bars are S.E.M. Significantly higher (*: P<0.05) degree of organization is observed for 60µm spacing compared to all other conditions. **(e-f)** Representative confocal images from OOP dataset, Blue: DAPI nuclei stain, White: α-actinin **(e)** x-y projection, scale-bars 10µm **(f)** x-z line scan. **(g)** Ratio between action potential (AP) propagation speed parallel and orthogonal to the

grooves for laminar NRVM tissue developed on substrates with 40, 60, 80 and 100μm filament spacing, ($n \geq 3$). Individual data points included (circles), error bars are S.E.M. The propagation speed of the action potential is faster in parallel than orthogonal to the grooves for all samples. The anisotropy in propagation speed is larger for tissue developed on 60μm spaced filaments than all other conditions. **(h)** Representative activation time maps for AP data set, overlaid wide field microscope image of the samples as guide to the eye, scale-bars 0.8mm. Activation times normalized to maximum observed activation (t_{max}), to account for tissue source variation. 2Hz electrical point-stimulation is applied in top left corner of samples. Mean observed propagation speed parallel (V_{para}) and orthogonal (V_{ortho}) to grooves is displayed as vectors. **(i)** Normalized AP traces at four corners of activation map samples. Blue: at AP initiation corner, Red: At t_{max}-corner, Black: Corner parallel to grooves, Green: Corner orthogonal to grooves.

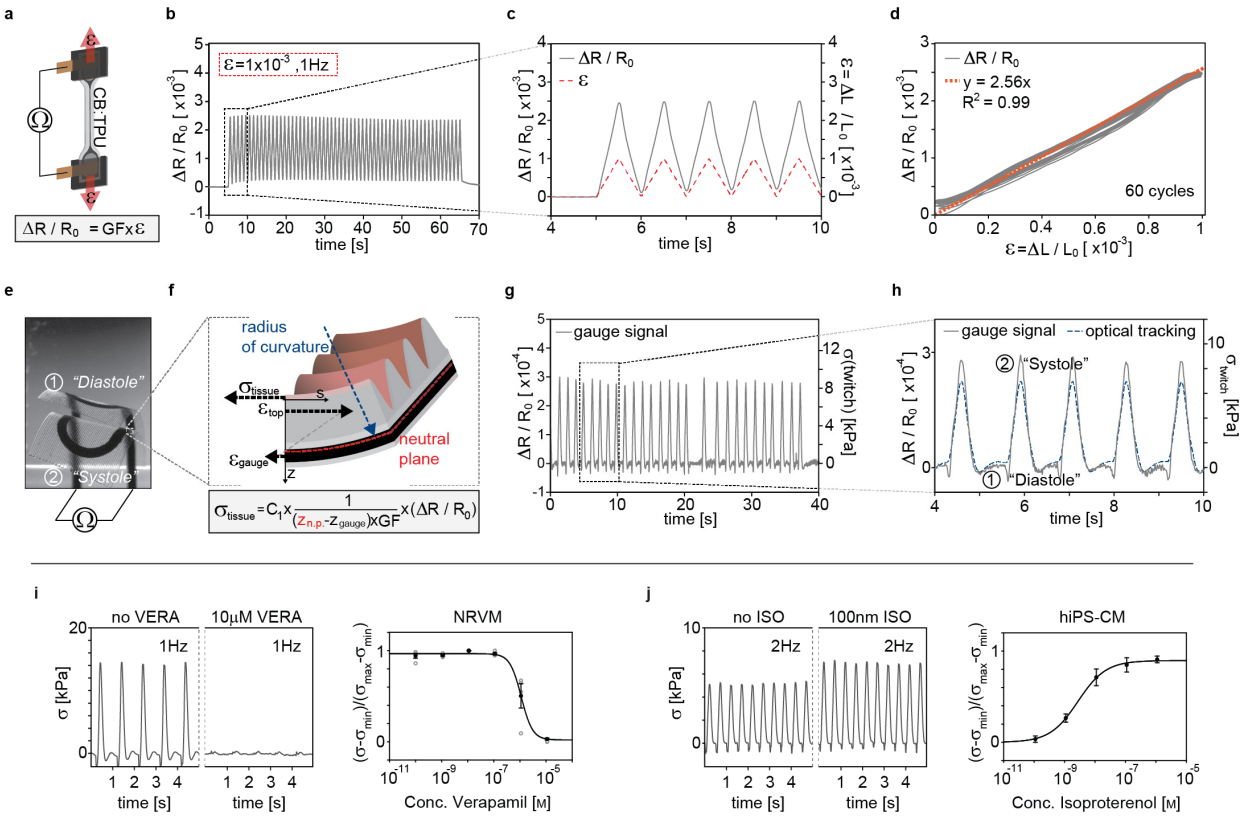

Figure 3 | CB:TPU gauge factor, sensor readout and example drug-dose studies. (a) Sketch of Instron test setup for determining CB:TPU gauge factor (GF). **(b-d)** Relative change in CB:TPU resistance upon triangular cyclic straining to 0.1% at 1Hz. **(c)** Dark grey line: Observed relative resistance change. Red dotted line: Strain applied. **(d)** Relative resistance change vs. applied strain. Orange dotted line indicates linear fit to part of cycles with increasing strain yielding a gauge factor of 2.56. **(e)** Wide-field microscope images of cantilever bending upon tissue contraction. Minimum deflection corresponds to cardiac diastole (1) and peak deflection corresponding to systole (2). **(f)** Sketch of mechanical model applied to convert resistance change to stress generated by the tissue, see Supplementary Inf. **(g-h)** Relative resistance changes (left axis) and corresponding calculated tissue stress (right axis) recorded from spontaneously beating cantilever. Blue dotted line in (h) indicates stress determined independently by optical tracking of the cantilever radius of curvature. **(i)** Representative traces

of stress generated by a laminar NRVM tissue when tissue is exposed to verapamil and corresponding dose-response curve (n=4), error bars are S.E.M, stress normalized between maximal and minimal values, tissue paced at 1Hz, apparent EC_{50} $1.12x10^{-6}$M. Individual data points included (circles) **(j)** Representative traces of stress generated by a laminar hiPS-CM tissue when exposed to isoproterenol and corresponding dose-response curve, (n=10), error bars are S.E.M, stress normalized between maximal and minimal values, tissue paced at 2Hz, apparent EC_{50} $2.74x10^{-9}$M.

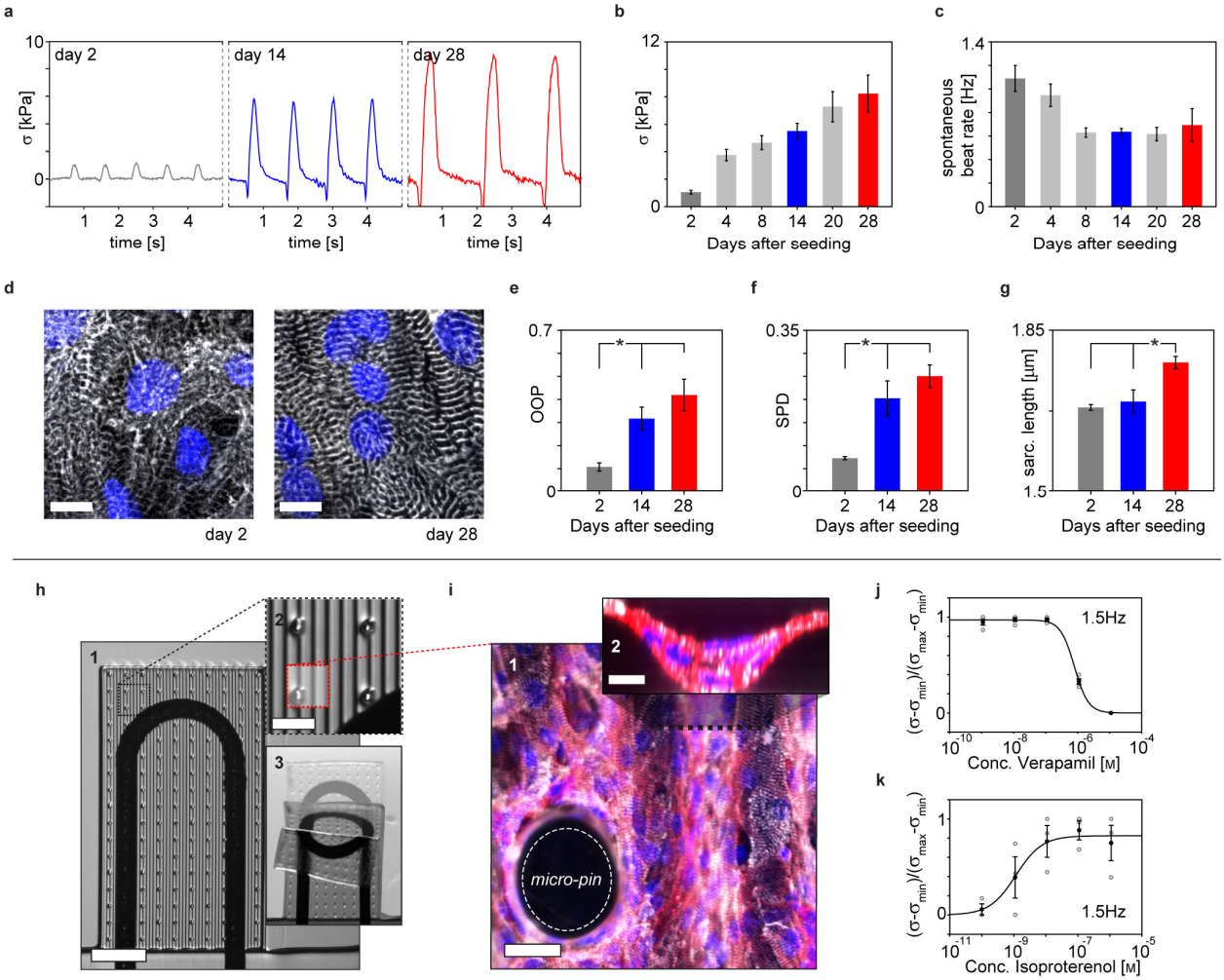

Figure 4 | Long term hips-CM contractile development and thicker laminar NRVM tissue devices (a) Representative traces of contractile twitch stress generated by the laminar hiPS-CMs tissues at day 2, 14 and 28 **(b-c)** Contractile stress and spontaneous beat rate of hiPS-CMs tissues at day 2, 4, 8, 20 and 28 (n≥10) error bars are S.E.M. **(d)** Immuno-stained laminar hiPS-CMs tissues on device cantilevers at day 2 and day 28 after seeding, scale bars 10µm. Blue: DAPI nuclei stain White: α-actinin stain, Z-projection **(e-g)** SPD, OOP and sarcomere length of laminar hiPS-CM tissues at day 2, 14 and 28 (n=5) error bars are S.E.M., *: P<0.05, **(h)** 1: Modified device cantilever containing micro-pin and micro-well to support thicker laminar NRVM tissue, 2: Detail of cantilever with micro-pins 3: Still images of a cantilever deflecting upon tissue contraction. **(i)** 1: Confocal microscopy Z-projection image of immuno-stained

thicker laminar tissue on the cantilever surface with micro-pin, scale bar 30μm. 2: Orthogonal image of thicker laminar tissue in depth of grooves, scale bar 10μm, Blue: DAPI nuclei stain, White: α-actinin, Red: actin. **(j)** Dose-response curve for verapamil, (n=4) for thicker laminar NRVM tissue, error bars are S.E.M. Individual data points included (circles), tissue paced at 1.5Hz. Stress values assumed linear proportional to relative resistance change: $\sigma \sim \Delta R/R_0$ and normalized between maximal and minimal values. Apparent EC_{50} 7.90×10^{-7}M **(k)** Dose-response curve for isoproterenol, for thicker laminar NRVM tissue, (n=3) error bars are S.E.M. Individual data points included (circles), tissue paced at 1.5Hz. Thicker tissue stress values assumed linear proportional to relative resistance change: $\sigma \sim \Delta R/R_0$. Stress normalized between maximal and minimal values. Apparent EC_{50} 1.16×10^{-9}M